Time-Resolved Cavity Ringdown Measurements and Kinetic Modeling of the Pressure Dependences of the Recombination Reactions of SiH_2 with the Alkenes C_2H_4, C_3H_6, and *t*-C_4H_8

Gernot Friedrichs,* Mustapha Fikri,† Yuanqing Guo,‡ and Friedrich Temps§

Institut für Physikalische Chemie, Olshausenstr. 40, Christian-Albrechts-Universität zu Kiel, D-24098 Kiel, Germany

Received: February 11, 2008; Revised Manuscript Received: April 4, 2008

Room-temperature rate constants for the pressure-dependent reactions SiH_2 + ethene, propene, and *t*-butene have been determined at total pressures of 3.3 mbar ≤ p ≤ 300 mbar with Ar as buffer gas. SiH_2 was detected by means of time-resolved cavity ringdown spectroscopy (CRDS), and the deconvolution of ringdown, kinetics, and laser bandwidth effect was accomplished with the extended simultaneous kinetics and ringdown model (eSKaR). In this way, pseudofirst-order rate constants could be extracted from nonexponential ringdown profiles. The recombination reactions, including the reaction SiH_2 + *i*-butene, have been modeled based on the simplified statistical adiabatic channel model (SACM) and weak collision energy-grained master equation (ME) simulations. The influence of an interfering fast isomerization channel was investigated based on the Rice, Ramsperger, Kassel, Marcus theory (RRKM) and was found to be only important for the C_2H_4 reaction. Using ab initio energies (G3) and structures (MP2/6-311G(d,p)) as input parameters for the kinetic models, a consistent description of the pressure and temperature dependences of all four reactions was possible. In the temperature range 295 K ≤ T ≤ 600 K, the extrapolated limiting high-pressure rate constants, $k_\infty(C_2H_4)/(cm^3 \cdot mol^{-1} \cdot s^{-1}) = 1.9 \times 10^{14}\ (T/K)^{-0.065}$, $k_\infty(C_3H_6)/(cm^3 \cdot mol^{-1} \cdot s^{-1}) = 1.3 \times 10^{14}\ (T/K)^{0.075}$, $k_\infty(i\text{-}C_4H_8) = 1.8 \times 10^{14}\ cm^3 \cdot mol^{-1} \cdot s^{-1}$, and $k_\infty(t\text{-}C_4H_8)/(cm^3 \cdot mol^{-1} \cdot s^{-1}) = 4.6 \times 10^{13}\ (T/K)^{0.21}$, are close to the collision number and are more or less temperature independent. In the case of ethene, probably due to the approximate treatment of rotational effects and/or the interfering isomerization process, the applied model slightly underestimates the falloff and thus yields too high extrapolated rate constants at p < 10 mbar.

1. Introduction

SiH_2 radicals are important intermediates in the chemistry of silicon hydrides and organosilicon compounds, and the reactions of SiH_2 with saturated and unsaturated hydrocarbons have practical significance for modeling chemical vapor deposition (CVD) processes.[1–3] In contrast to CH_2, for which the chemistry is complicated by the interplay of a less reactive triplet ground state and an energetically low-lying reactive singlet state, SiH_2 reactions are dominated by its singlet ground state ($^1A_1$).[4] A considerable set of SiH_2 reaction rate constants, mostly based on time-resolved measurements of SiH_2 concentration profiles, already exist and have been reviewed by Walsh and co-workers[5,6] and more recently were updated and compared with available data for other heavy carbenes by Becerra and Walsh.[7] As can be expected for a singlet radical, the reactions of SiH_2 with hydrocarbons are mostly C−H bond insertion and C=C π-bond addition processes.

The addition reaction of SiH_2 to the π-bond can be described as a two-stage process with an electrophilic stage, where π electrons are donated to the empty p orbital of SiH_2, followed by a nucleophilic stage with the lone pair of the SiH_2 interacting with the antibonding π^* orbital of the alkene double bond.[5] Temperature- and pressure-dependent rate constant measurements of the reactions of SiH_2 with ethene, propene, and *i*-butene have shown that the addition reactions (i) show a pronounced pressure dependence (falloff) over the range 1 Torr < p < 100 Torr, (ii) proceed close to their collisional limits, and—based on high-pressure extrapolations of the rate constants— (iii) the reactions are only slightly temperature dependent with negative activation energies of $-E_a = (2-3)$ kJ/mol.[8,9] In agreement with these findings, the SiH_2 addition reactions were interpreted to constitute simple third-body mediated association processes forming siliranes according to

$$SiH_2 + H_2C{=}CXY + M \rightarrow H_2Si\langle \begin{matrix} CH_2 \\ | \\ CXY \end{matrix} + M \qquad (1)$$

with X,Y = H or CH_3, respectively. Assuming that there are no other perturbing reaction channels, the observed pressure dependences of the association reactions correspond to the pressure dependences of the reverse unimolecular decomposition reactions of the silirane rings. The modeling of such simple bond fission (dissociation) reactions is hampered due to the fact that no common (*tight*) transition state can be defined. Moreover, to account for the loose structure of the transition state, the transformation of some oscillators of the silirane into product rotors and adiabatic angular momentum effects have to be properly taken into account for the calculation of J-dependent specific rate constants $k(E, J)$. Variational RRKM models with hindered rotor treatments[10] or, alternatively, a simplified SACM model where channel states are interpolated between reactant

* E-mail address: friedrichs@phc.uni-kiel.de.
† Present address: Institut für Verbrennung and Gasdynamik, Lotharstr. 1, Universität Duisburg-Essen, D-47057 Duisburg, Germany.
‡ Present address: Department of Chemistry, Colorado State University, Fort Collins, CO 80523-1872.
§ E-mail address: temps@phc.uni-kiel.de.

10.1021/jp8012128 CCC: $40.75
Published on Web 05/31/2008

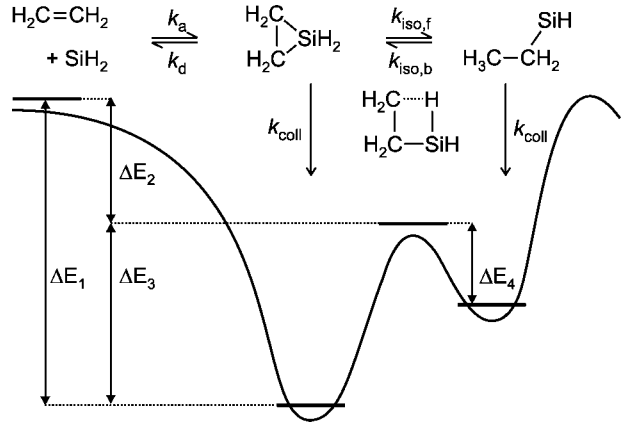

Figure 1. Schematic potential energy diagram of the association reactions SiH_2 + alkenes with C_2H_4 as an example. Barrier energies (including zero point energies) are listed together with typical values of the specific rate constants *k* for the association (index a), dissociation (d), forward and backward isomerization (iso,f and iso,b), and collisional deactivation (coll) processes in Table 2.

and product eigenvalues[11] have been proven to allow for rational and accurate modeling of bond fission reactions.

In a straightforward manner, Walsh and co-workers performed RRKM calculations on SiH_2 + alkene reactions with input parameters estimated from an iterative fitting procedure of the observed falloff curves. In short, vibrational frequencies of the transition states were assigned by adjusting (lowering) the frequencies of the ring modes and the SiH_2 group vibrations until a match was obtained with the entropies of activation (estimated from thermochemical calculations) and the Arrhenius *A* factors of the association reactions. *A* factors were obtained by extrapolating the falloff curves to infinite pressures based on a weak collision stepladder model for collisional deactivation. Whereas a variational character of the transition state was implicitly taken into account by using modified transition state frequencies at each temperature, rotational effects were neglected in their analysis. Using the critical energy E_0 as the main adjustable parameter, good agreement between experimental and theoretical temperature- and pressure-dependent rate constant data could be established in all cases.

The simple association model according to eq 1 is challenged by ab initio calculations of the potential energy surface. These calculations clearly show that the initially formed three-membered silirane ring can undergo reversible ring opening processes (retrograde C−H insertion) to form alkylsilylenes.[12,13] A scheme of the resulting potential energy diagram is shown with ethylene as an example in Figure 1. The silirane/alkylsilylene isomerization takes place over an energetically low-lying *tight* transition state with an energy barrier that is approximately 75 kJ/mol lower than the critical energy of the silirane decomposition process. In general, such a low-lying alternative exit channel cannot be neglected for theoretical modeling of the overall association rate constant. Subsequent further isomerization of the alkylsilylenes into 2-alkylsilenes ($H_2Si{=}CH{-}CH_3$ in the case of ethylene) is also feasible. However, the respective energy barriers are comparable to the entrance energies of the reactants such that these isomerizations—due to the much lower specific rate constant values associated with the *tight* transition states—do not play a role. Other possible processes, e.g., ring opening to diradical structures or isomerization into 1-alkylsilene, are discussed by Skancke et al.[13] and Sengupta and Nguyen[12] but can be also neglected due to energetic reasons. According to this, the association process can be described as follows: The initial formation of the highly excited silirane association complex is followed by a rapid isomerization and equilibration with the alkylsilylene isomerization product. Next to the redissociation of the silirane complex into reactants, both the silirane and the alkylsilylene can be collisionally deactivated to form stable products. Actually, there is strong experimental confirmation of this fast isomerization process. Al-Rubaiey et al.[14] investigated the temperature and pressure dependence of the rate constant of the reaction SiH_2 + C_2D_4 by measuring SiH_2 concentration−time profiles. A comparison with the corresponding SiH_2 + C_2H_4 rate constants (apparently) revealed a much less distinctive pressure dependence for the deuterated alkene that could not be attributed to an isotopic effect alone. In fact, due to the fast equilibration of the silirane-d_4 with its open ethylsilylene-d_4 isomers, an isotope scrambling process occurs, and dissociation of the resulting diverse d_4-siliranes next to SiH_2 also yields SiHD and SiD_2. In this way, the isomerization process acts as an efficient sink for SiH_2 such that the experimentally measured SiH_2 decay profiles at low pressures were dominated by this isotope scrambling process rather than silirane deactivation.

The aim of this study was 3-fold. First of all, the experimental data pool on SiH_2 + alkene rate constant data was expanded by room-temperature measurements on ethene, propene, and (for the first time) *t*-butene. SiH_2 concentration−time profiles were measured by means of cavity ringdown spectroscopy (CRDS) under pseudofirst-order conditions with the concentrations of the alkenes in large excess over SiH_2. The experimental total pressures were varied over a wide range, 3.3 mbar < p < 300 mbar, to facilitate accurate extrapolations of the limiting high-pressure rate constants. Second, the silirane/alkylsilylene isomerizations were modeled by RRKM theory to elucidate a possible role of the fast equilibration process, and third, it was tested whether SACM calculations, which were rigorously based on ab initio input parameters, result in a consistent modeling of the recombination rate constants. In this context, the anisotropy (or looseness) parameter α (or the anisotropy ratio α/β, SACM model) and the average energy removal parameter $\langle\Delta E_{down}\rangle$ (master equation modeling) were used as the sole adjustable parameters to fit the high-pressure limiting rate constant and the falloff curvature, respectively. Finally, the performance of the model was evaluated by a detailed comparison of the model predictions with existing literature data.

2. Experimental Section

SiH_2 radicals were detected by means of cavity ringdown spectroscopy (CRDS). As a sensitive and quantitative absorption-based detection method, CRDS has been widely used in gas-phase reaction kinetics.[16] The cavity ringdown setup used in the present work is similar to that used in our previous studies on SiH_2 and NH_2 reactions.[15,18] A 1 m long resonant optical cavity was formed by two highly reflective mirrors with 6 m radii of curvature, which were held in adjustable mounts attached to a quartz flow tube via flexible bellows. The output of a Nd:YAG pumped tunable dye laser (Quanta Ray PDL-3, 9 ns pulse length) was shaped and spatially filtered by two telescopes and a 50 μm pinhole before it was injected into the cavity as the ringdown probe laser. The light intensity decay, the so-called ringdown, was monitored by a photomultiplier, low-pass-filtered at 10 MHz, and stored in an 8 bit digital oscilloscope with summed averaging. Without an absorber in the cavity, the ringdown curves were found to be single-exponential with a measured empty cavity ringdown time of $\tau_0 \approx 25$ μs. Typically,

TABLE 1: Experimental Conditions and Determined Rate Constants k (SiH_2 + Alkene) and k_d (Background Reactions and Diffusion Loss)[a]

reactant	p / mbar	$[PhSiH_3]_0$ / (10^{-11} mol/cm^3)	$[C_2H_4]_0$ / (10^{-9} mol/cm^3)	k / (10^{13} cm^3·mol^{-1}·s^{-1})	k_d / (10^4 s^{-1})
C_2H_4	4.2	2.1	0.9−5.3	3.6 ± 0.3	−1.2 ± 1.0
	6.0	2.9	2.7−7.6	3.9 ± 0.4	2.2 ± 2.2
	6.0	3.0	2.7−12	3.0 ± 0.5	1.1 ± 4.1
	10	1.8	0.6−2.5	5.0 ± 0.4	0.8 ± 1.2
	15	2.7	0.6−8.9	4.5 ± 0.9	3.3 ± 4.5
	15	1.8	1.3−8.0	4.7 ± 0.6	3.3 ± 4.6
	20	2.8	0.3−2.5	7.6 ± 0.4	1.6 ± 0.6
	30	3.0	0.5−3.2	9.1 ± 1.4	1.5 ± 2.8
	40	3.0	0.6−2.4	7.2 ± 0.9	3.8 ± 1.4
	60	3.0	0.4−2.2	7.8 ± 0.8	3.3 ± 1.4
	80	3.0	0.5−2.9	8.9 ± 0.9	3.3 ± 1.7
	100	3.0	0.6−2.4	10.7 ± 3.3	0.8 ± 5.5
	150	6.0	0.6−4.0	10.3 ± 1.4	12.7 ± 3.2
	200	6.0	0.4−4.6	12.2 ± 1.9	20.7 ± 4.5
	300	9.0	0.6−2.9	9.7 ± 0.7	11.3 ± 1.2
C_3H_6	6	2.1	0.4−2.8	6.5 ± 0.9	5.0 ± 1.5
	10	2.1	0.5−2.8	7.7 ± 1.7	5.0 ± 1.5
	15	2.1	0.4−2.5	9.2 ± 1.3	6.3 ± 3.3
	15	2.1	0.2−1.0	11.1 ± 0.7	6.5 ± 1.8
	20	2.1	0.3−1.5	11.3 ± 2.0	5.0 ± 0.4
	30	2.1	0.8−2.7	13.4 ± 1.3	5.0 ± 2.2
	30	2.1	0.2−1.9	13.7 ± 1.4	4.4 ± 2.5
	60	2.1	0.4−1.5	12.4 ± 3.2	7.8 ± 1.6
	80	2.1	0.4−1.9	15.3 ± 4.2	9.8 ± 3.3
	100	2.1	0.3−2.0	16.2 ± 2.2	10.1 ± 3.8
	200	2.1	0.4−2.2	15.9 ± 4.3	4.8 ± 6.2
	300	2.1	0.6−2.8	16.5 ± 3.1	−1.8 ± 5.7
t-C_4H_8	3.3	2.1	0.2−0.5	5.8 ± 1.6	0.9 ± 0.6
	4.9	2.1	0.1−0.4	8.4 ± 1.5	1.3 ± 0.5
	10	2.1	0.3−1.4	10.8 ± 0.8	2.1 ± 0.7
	20	2.1	0.3−1.1	11.2 ± 2.3	4.7 ± 1.7
	30	2.1	0.3−1.4	10.5 ± 2.5	3.2 ± 2.2
	30	2.1	0.3−1.1	10.4 ± 1.6	3.4 ± 1.3
	40	2.1	0.1−0.6	12.6 ± 1.1	2.2 ± 0.5
	80	2.1	0.3−1.5	12.7 ± 1.6	5.3 ± 1.6
	120	2.1	0.3−1.4	13.2 ± 1.5	4.0 ± 1.4
	200	2.1	0.2−1.2	13.7 ± 2.1	5.9 ± 1.5
	300	2.1	0.2−1.2	13.8 ± 1.9	3.2 ± 1.1

[a] All experiments were performed at room temperature, $T = 295$ K. A time delay of $\Delta t \approx 3$ μs between firing the photolysis laser and the probe laser was introduced to ensure complete relaxation of the initially formed rovibrationally excited SiH_2 radicals. Initial $[SiH_2]_0$ concentrations are about 2−3% of the $[PhSiH_3]_0$ concentrations. The indicated errors correspond to 2σ errors of the linear least-squares fits of the pseudofirst-order rate constant data (see also Figure 4).

20 ringdown decays were averaged and then transferred to a personal computer for data analysis in real-time. An ArF excimer laser (Lambda Physik Compex 102, 15 ns pulse duration, 10 Hz repitition rate) was used to generate SiH_2 radicals by photolysis of phenylsilane at $\lambda = 193$ nm according to[17]

$$PhSiH_3 + h\nu \rightarrow SiH_2 + C_6H_6 \quad (2a)$$

$$\rightarrow PhSiH + H_2 \quad (2b)$$

To increase the spatial overlap between the photolysis and the probe laser, the photolysis beam (1.5 × 3.0 cm^2 cross section) was passed through the flow tube at an angle of 20 degrees with respect to the cavity axis resulting in a single and effective absorption path length of 8.8 cm and 660 m, respectively. In most kinetic experiments, the initial phenylsilane concentration was set to $[PhSiH_3]_0 = 2.1 \times 10^{-11}$ mol/cm^3. Based on the reported absorption cross section at $\lambda = 193$ nm ($\sigma \approx 2.3 \times 10^7$ cm^2/mol),[17] the reported quantum yield for SiH_2 formation ($\varphi_{2a} \approx 0.15$),[17] and an average laser energy of 40 mJ/pulse, the initial SiH_2 concentration can be estimated to be $[SiH_2]_0 \approx 9 \times 10^{-13}$ mol/cm^3.

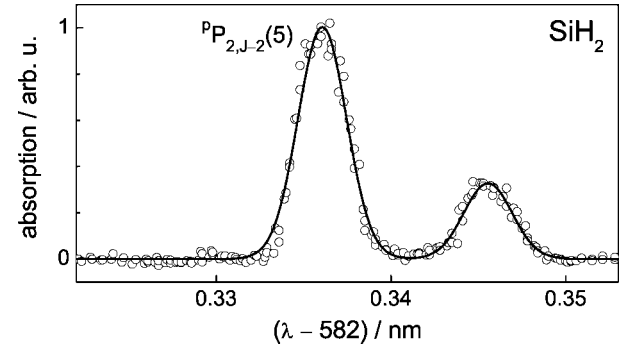

Figure 2. High-resolution CRD scan over the $^pP_{2,J-2}(5)$ rotational line at $\lambda = 582.336$ nm (circles). To minimize pressure broadening and the influence of the laser bandwidth effect, the measurement was performed at a low pressure of $p = 2.5$ mbar and at overall low SiH_2 absorption. The solid curve corresponds to a Gaussian fit with an effective spectral line width of $\Delta\tilde{\nu} = 0.095$ cm^{-1}.

Figure 2 illustrates a high-resolution scan over the rotationally resolved $^pP_{2,J-2}(5)$ line of the $\tilde{A}\ ^1B_1$ (020) ← $\tilde{X}\ ^1A_1$ (000) SiH_2 transition at $\lambda = 582.336$ nm, which was used for SiH_2 detection

in all kinetic experiments. This measurement was performed at a low pressure of $p = 2.5$ mbar and at overall low SiH_2 absorption. Moreover, the fit of the ringdown curve was restricted to the region $1 \geq I/I_0 \geq 0.85$ (I is the detected light intensity). Whereas at low pressures the observed line shape is dominated by the convolution of the probe laser line width with the SiH_2 Doppler broadened absorption line width ($\Delta\tilde{\nu}_{Doppler} = 0.0385\ cm^{-1}$), low overall SiH_2 absorption and a restricted fit range is important to minimize line shape distortions due to the probe laser bandwidth effect. This laser bandwidth effect, which is observed when the probe laser line width is comparable to or exceeds the absorption line width of the detected species (as it is a common situation when detecting small radicals with pulsed dye lasers), causes nonexponential ringdown signals, and thus complicates a simple single-exponential ringdown analysis. The effect is discussed in some length in our previous papers and can be properly taken into account by a forward modeling procedure.[16,18] In Figure 2, the solid curve corresponds to a fit of the experimentally observed line shape assuming a Gaussian probe laser line width of $\Delta\tilde{\nu}_{laser} = (0.087 \pm 0.004)\ cm^{-1}$. Similarly, the pressure broadening coefficient of the probed SiH_2 line was determined from line shapes measured at $p = 300$ mbar to be $1.4 \times 10^{-4}\ cm^{-1}\ mbar^{-1}$. Although both the probe laser and absorption line shape have to be known to evaluate kinetic ringdown curves based on the eSKaR model (see Section 3), we have shown in our previous publications that small line shape inaccuracies induce practically negligible errors in the finally determined rate constants.[15,18]

Gas mixtures were prepared manometrically and were stored in glass flasks. The actual reaction gas mixtures with the desired $[PhSiH_3]$/[alkene] ratios were prepared from the storage mixtures and were further diluted with Ar by using a flow system with calibrated mass flow controllers (AERA, FC series). The total pressure in the ringdown cavity was measured by a capacitance manometer (MKS 622A), and the flow speed in the reactor (10 to 30 cm/pulse) was kept fast enough to avoid repeated photolysis of the same gas volume. Gases and chemicals used used were Ar (99.999%), ethene (99.995%), propene (99.98%), *t* -butene (98%), and degassed phenylsilane (97%).

3. Results

The pressure dependences of the addition reactions of SiH_2 with the alkenes ethene, propene, and *t*-butene

$$SiH_2 + H_2C{=}CH_2 + M \rightarrow H_2Si\langle \begin{matrix} CH_2 \\ | \\ CH_2 \end{matrix} + M \quad (3)$$

$$SiH_2 + H_2C{=}CH\text{-}CH_3 + M \rightarrow H_2Si\langle \begin{matrix} CH\text{-}CH_3 \\ | \\ CH_2 \end{matrix} + M \quad (4)$$

$$SiH_2 + H_3C\text{-}HC{=}CH\text{-}CH_3 + M \rightarrow H_2Si\langle \begin{matrix} CH\text{-}CH_3 \\ | \\ CH\text{-}CH_3 \end{matrix} + M \quad (5)$$

have been investigated at room temperature and pressures between 3.3 mbar $\leq p \leq$ 300 mbar under pseudofirst-order conditions with a large excess of the alkenes ($110 \leq$ [alkene]$_0$/[SiH_2]$_0 \leq$ 10 370). Following the photolysis of phenylsilane/alkene mixtures in Ar, the characteristic reaction times for SiH_2 loss were in the range of 10 μs and thus occurred on the same time scale as the ringdown. Consequently, nonexponential ringdown curves were observed due to the convolution of probe light decay and concentration change. Moreover, due to the finite spectral bandwidth of the probe laser, the so-called laser bandwidth effect arises causing the observed ringdown curves to be nonexponential even in the case of constant absorber concentration. Therefore, the determination of rate constant data from nonexponential ringdown curves requires the deconvolution of the kinetics and the bandwidth effect. Recently, we presented an extended version (eSKaR) of the simultaneous kinetics and ringdown model (SKaR) of Brown et al.[19] that has been shown to provide a reliable method for extracting rate constants from ringdown profiles with interfering laser bandwidth effect.[15,18] Within this model, the temporal behavior of the measured ringdown curve is described by a summation (or integration) over all signal contributions stemming from different excited optical modes in the ringdown cavity. In the case of a dense mode spectrum, the ratio of the time-dependent intensities measured with absorber, $I(t)$, and measured without absorber, $I_0 \times \exp(-t/\tau_0)$, is given by[16]

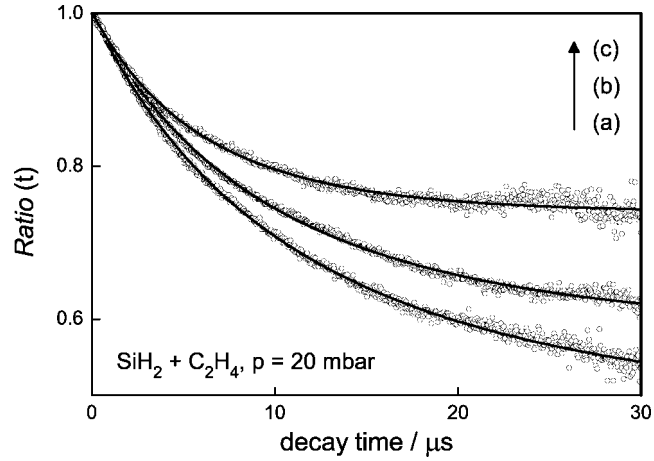

Figure 3. Experimental Ratio(t) curves (open circles) and corresponding eSKaR fits at three different initial concentrations of C_2H_4. (a) $[C_2H_4]_0 = 3.1 \times 10^{-10}$ mol/cm^3, (b) 6.2×10^{-10} mol/cm^3, (c) 1.54×10^{-9} mol/cm^3. Experimental conditions: $[PhSiH_3]_0 = 2.8 \times 10^{-11}$ mol/cm^3, $[SiH_2]_0 \approx 1.2 \times 10^{-12}$ mol/cm^3, $p = 20$ mbar, $T = 295$ K.

$$\text{Ratio}(t) = \frac{I(t)}{I_0 \exp(-t/\tau_0)} = \int_{+\infty}^{+\infty} g_{laser}(\nu - \nu_c) \exp\left(-\frac{c\alpha_{c0} l g_{abs}(\nu - \nu_c)}{k' L}(1 - e^{-k't})\right) d\nu \quad (6)$$

Here, I_0 and α_{c0} are the light intensity and the narrow-bandwidth (line center) absorption coefficient measured at $t = 0$; c is the speed of light; l is the single path absorption length (8.8 cm); L defines the length of the cavity (1 m); and τ_0 corresponds to the empty cavity ringdown time. $g_{laser}(\nu - \nu_c)$ and $g_{abs}(\nu - \nu_c)$ represent the line shape functions of the probe laser (Gaussian profile) and the absorption line (Voigt profile), respectively, and have been determined separately as described in the experimental section. A first-order kinetics has been assumed for the derivation of eq 6, and k' corresponds to the first-order (or pseudofirst-order) rate constant. In the kinetic experiments, the probe laser was step-scanned over the SiH_2 absorption line, and all ringdown data were saved on the computer. From these data, two ringdown curves corresponding to on-resonance (line-center absorption) and off-resonance (empty cavity signal) were selected for further analysis. Furthermore, to make sure simple first-order kinetics, a time delay of $\Delta t = 1-5$ μs (depending on the total pressure) was introduced between firing the photolysis laser and the probe laser to ensure relaxation of the initially formed rovibrationally excited SiH_2 radicals.[15] In Figure 3, typical Ratio(t) curves (open

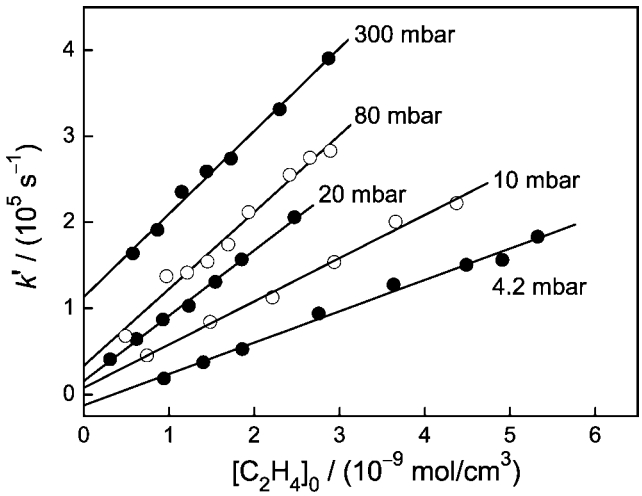

Figure 4. Pseudofirst-order rate constant $k' = k_3 \times [C_2H_4]_0 + k_d$ as a function of the concentration of C_2H_4. Experimental conditions are given in Table 1.

circles) are shown for three experiments with increasing ethene concentrations at $p = 20$ mbar together with the corresponding eSKaR fits (solid curves). Using the absorption coefficient α_{c0} and the pseudofirst-order rate constant as the fitting parameters, very good agreement of the eSKaR fit with the experimental data was obtained in all cases. As can be shown from eq 6, the two limiting cases of very short and very long decay times allow for a partially decoupled determination of the two fitting parameters. At short times, the initial decrease of the Ratio(t) signal is independent of the rate parameter k', whereas the plateau value observed at long times is determined by the ratio of α_{c0} and k'.[16] The higher plateau values seen for increasing ethene concentrations in Figure 3 directly reflect the faster SiH_2 removal rate.

The determined rate constants k' are plotted as a function of the ethene concentration in Figure 4 and, as can be expected for a pseudofirst-order reaction, show a linear dependence on $[C_2H_4]_0$. Second-order rate constants k_3 were obtained by a linear fit of the data according to $k' = k_3 \times [C_2H_4]_0 + k_d$. Selected data sets for five different pressures, $p = 4.2$, 10, 20, 80, and 300 mbar, are shown. The increase of the slopes of the best fit straight lines with increasing pressure reflects the pressure dependence of the overall rate constant. The intercept k_d is correlated to the initial phenylsilane concentration and is caused by SiH_2 background losses mainly attributable to reactions of SiH_2 with the unphotolyzed precursor[17] and, to a lesser extent, also to diffusion loss. Both background loss components can be assumed to be independent of the alkene concentration and thus, despite the relatively high values of k_d, do not interfere with the second-order rate constant determination. Note that inaccuracies in the assumed line shape model give rise to apparent intercept values as well but have only a minor influence on the extracted second-order rate constant.[15,18] In Table 1, a complete list of the determined pressure-dependent bimolecular rate constants and the corresponding intercept values is given for the reactants ethene, propene, and t -butene. On average, each bimolecular rate constant is based on 6−7 measurements with varied alkene concentrations, and Table 1 summarizes the results of some 250 single measurements. The specified error limits correspond to the 2σ uncertainty of the linear regression. Overall, within the relatively large scatter of the determined intercept values, no clear systematic trend of k_d with pressure is discernible. In contrast, as can be seen from the double-logarithmic plot of the bimolecular rate constant versus total pressure in Figure 5 (falloff plot), for all three alkenes, a pronounced pressure dependence of the SiH_2 removal rate constant is evident. Values of $(1-2) \times 10^{14}$ cm^3·mol^{-1}·s^{-1} obtained for the rate constants at the highest experimental pressure of $p = 300$ mbar are close to the collision number Z_{coll}, and hence a reliable extrapolation of the limiting high-pressure rate constants, $k_\infty \leq Z_{coll}$, is feasible.

4. Theoretical Modeling. The addition reactions of SiH_2 radicals to alkenes proceed on potential energy surfaces similar to the one shown for ethene in Figure 1. The initially formed three-membered silirane ring can undergo a reversible ring-opening step to form alkylsilylenes. For kinetic modeling of the overall addition rate constant in the framework of statistical theories (SACM, variational RRKM), the energies and structures of the reactants, intermediates, and products have to be known. Model input parameters were obtained from ab initio calculations on the MP2/6-311G(d,p) and the G3 levels of theory using the program suite Gaussian 03.[20,21] In Table 2, G3 energy barriers as specified in Figure 1 are listed for the alkenes ethene, propene, *i*-butene, and *t*-butene. Although not measured in this work, all calculations were also performed on the reaction with *i*-butene

$$SiH_2 + H_2C{=}C\text{-}(CH_3)_2 + M \rightarrow H_2Si\langle \begin{matrix} C\text{-}(CH_3)_2 \\ | \\ CH_2 \end{matrix} + M \qquad (7)$$

to allow for a comparison with literature data. An average ΔE_2 value of 6300 cm^{-1}, which was estimated from calculated MP2 energies of the isomerization transition states according to $\Delta E_2(G3) \approx \Delta E_1(G3)/\Delta E_1(MP2) \times \Delta E_2(MP2)$ was used in all RRKM calculations. A complete list of the calculated energies and the structures of the transition states is given in the Supporting Information. With increasing alkyl substitution of the alkene, due to an increase of the ring strain energy, the decomposition barrier of the siliranes, ΔE_1, decreases from 14 900 cm^{-1} (178 kJ/mol) in the case of ethene to 13 600 cm^{-1} (163 kJ/mol) in the case of t -butene. For all alkenes, the open alkylsilylene is much less stable than the silirane ring structure by $\Delta E_3 - \Delta E_4 \approx 5200$ cm^{-1} (62 kJ/mol) such that the siliranes can be assumed as the predominant product of the addition reaction.

To assess a possible influence of the fast isomerization process, specific (microcanonical) rate constants $k_{iso,f}(E)$ and $k_{iso,b}(E)$ were calculated using home-written software[22] based on standard RRKM calculation procedures.[10,23] All low-wavenumber vibrations associated with torsional rotations of the alkyl groups were treated as internal rotors. Although (external) rotational effects are less important for isomerization processes with tight transition states, rotationally resolved specific rate constants $k(E, J)$ were calculated first but were averaged over the rotational distribution as will be discussed in more detail below.

RRKM parameters for 2-methylsilirane and propylsilylene are listed in Table 3. Note that all structural parameters were taken from the MP2 calculations and that the vibrational frequencies have been slightly scaled by a factor of 0.9496 taken from Scott and Radom.[24] Similarly, $k_d(E)$ values have been calculated for the barrierless bond fission (dissociation) reaction with loose transition state based on the simplified SACM model according to Quack and Troe.[11,25,26] The required correlation scheme of conserved and disappearing oscillators was based on a detailed vibrational analysis and is outlined for 2-methylsilirane in Table 4. Corresponding RRKM and SACM input parameters for all other alkenes can be found in the Supporting

TABLE 2: Energy Barriers, Specific Rate Constants $k(E)$ of Dissociation (d), Forward and Backward Isomerization (iso, f and iso, b), and Collisional Deactivation Rate Constants (coll, $p = 10$ mbar Ar, $T = 295$ K)[a]

reactant	ΔE_1	ΔE_2	ΔE_3	ΔE_4	k_{coll}	E_{int}	$k_d(E_{int})$	$k_{iso,f}(E_{int})$	$k_{iso,b}(E_{int})$	x_{cycl}
C_2H_4	14897	6300	8597	3567	1.0×10^8	15133	6.6×10^7	1.2×10^{10}	3.5×10^{10}	0.74
						8863		1.4×10^7	2.7×10^8	0.95
C_3H_6	14223	6300	7923	2844	1.1×10^8	14743	2.2×10^7	7.3×10^8	4.7×10^{10}	0.98
						8473		5.6×10^5	2.3×10^8	>0.99
i-C_4H_8	13888	6300	7588	2381	1.2×10^8	14678	1.6×10^6	3.9×10^8	9.5×10^9	0.96
						8408		2.2×10^5	1.4×10^8	>0.99
t-C_4H_8	13596	6300	7296	1882	1.2×10^8	14424	3.0×10^6	1.0×10^9	2.3×10^{10}	0.96
						8154		6.5×10^5	5.3×10^8	>0.99

[a] For the notation of the energy barriers see Figure 1. E_{int} is the internal energy of the silirane and alkylsilylene isomers and $x_{cycl} = k_{iso,b}/(k_{iso,b} + k_{iso,f})$ is the corresponding steady-state fraction of the excited silirane recombination product. Energies are given in units of cm^{-1} and rate constants in units of s^{-1}.

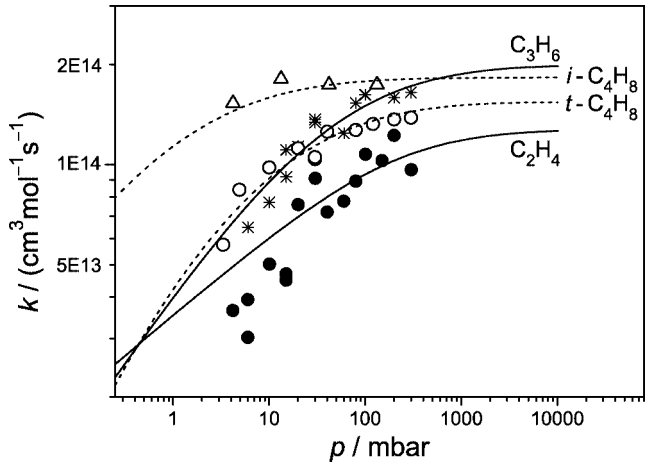

Figure 5. Experimental room-temperature rate constant data for the reactions SiH_2 + alkenes in comparison with kinetic modeling results. (●) C_2H_4 (Ar, $T = 295$ K, this work); (∗) C_3H_6 (Ar, $T = 295$ K, this work); (○) *t*-C_4H_8 (Ar, $T = 295$ K, this work); (Δ) *t*-C_4H_8 (SF_6, 298 K, Al-Rubaiey and Walsh).[8]

Information. Finally, the Lennard-Jones collision frequencies were calculated based on collision diameters estimated from Le Bas increments for the molar volumes using the relationship $\sigma = 1.18V_b^{1/3}$ and potential well depths using the relationship $\varepsilon/K = 1.21T_b$.[27,28] T_b values were estimated based on a systematic shift in boiling points, $T_b(Si) \approx T_b(C) + 25$ K, found for many analogous Si and C compounds.

Table 2 compares specific rate constants $k(E)$ of the dissociation and forward and backward isomerization steps with the room temperature collisional deactivation rate constants k_{coll} at a total Ar buffer gas pressure of $p = 10$ mbar. k_{coll} values are given in units of s^{-1} such that the collisional deactivation rate constant is dependent on the total pressure. In thermal average, vibrationally excited silirane complexes are formed with internal energies of $E_{int} = \Delta E_1 + E_{thermal}$, and a set of specific rate constants referring to these internal energies is listed in Table 2. To assess the energy dependence of the isomerization process, another set of rate constants corresponding to a value of E_{int} close to the silirane/alkylsilylene isomerization barrier is also specified. On one hand, in all four cases $k_{coll} \gtrsim k_d$ such that the collisional deactivation competes successfully with the dissociation. Especially for the butenes, with $k_{coll}/k_d \approx 50$, the reaction proceeds already close to the high-pressure limit at $p = 10$ mbar. On the other hand, the comparison of the dissociation and isomerization rate constant data reveals that the isomerization process is indeed much faster than the dissociation of the initially formed silirane complex. Hence a fast (microcanonical) equilibrium of the siliranes with the corresponding alkylsilylenes is established. The steady-state fractions of the cyclic silirane complexes are given by $x_{cycl} = k_{iso,b}/(k_{iso\,b} + k_{iso,f})$ and are also listed in Table 2. In all cases, the dependence of of x_{cycl} on E_{int} is weak, and the value corresponding to the internal energy of the initially formed excited complexes can be taken as a good measure to infer the influence of the isomerization process on the kinetic modeling. For propene, *i*-butene, and *t*-butene, x_{cycl} is close to 1 such that the relative population of the alkylsilylene energy states remains small. Consequently, the isomerization process can be neglected, and the temperature and pressure dependence of the overall addition reaction can be modeled as a simple recombination reaction. Only in the case of ethene, with $x_{cycl} = 0.74$, the ethylsilylene has to be taken into account. The main effect is that a smaller fraction of the silirane complex is available for dissociation into the reactants. Assuming an extended Lindemann−Hinshelwood mechanism as outlined in Figure 1, the overall recombination rate constant including the isomerization process is given by

$$\frac{k}{k_\infty} = 1 - \frac{k_d \times x'}{k_d \times x' + k_{coll}} \quad (8)$$

$$x' = \frac{k_{iso,b} + k_{coll}}{k_{iso,b} + k_{iso,f} + k_{coll}} \quad (9)$$

Figure 6 illustrates a calculated falloff curve based on this (canonical) extended Lindemann−Hinshelwood model using the (microcanonical) rate constant data set for ethene taken from Table 2 (circles). A comparison with the falloff curve obtained for a simple recombination model neglecting isomerization (dashed curve, $x' = 1$) reveals that the overall effect of the isomerization is a shift of the fall-curve to lower pressures. At low pressures and/or fast isomerization, k_{coll} can be neglected in eq 9 such that $x' = x_{cycl}$. For ethene, there is nearly perfect agreement of such an approximate falloff curve (solid curve) with the falloff curve corresponding to the complete Lindemann−Hinshelwood treatment. Note that for slower isomerization processes this simple procedure would yield increasingly too high rate constants in the falloff range. However, for recombination reactions with a fast interfering isomerization step, accurate modeling is possible based on a simple recombination model by taking the isomerization step into account by simply replacing $k_d(E)$ with the effective dissociation rate constant $k_d(E) \times x_{cycl}$. An alternative but similar approach would be to calculate $k_d(E)$ based on the sum of the densities of states of the silirene and the alkylsilylene instead of the density of states of the silirane alone. In both ways, accurate falloff curves for the overall recombination reaction can still be obtained based on a standard statistical treatment of the reverse unimolecular dissociation process. Of course, the high-pressure limiting recombination

TABLE 3: RRKM Parameters for Isomerization of 2-Methylsilirane to Propylsilylene and Vice Versa[a]

	$CH_3-C_2SiH_5$	$[CH_3-C_2SiH_5]^‡$	$CH_3-C_2H_4-SiH$
critical energy, E_0/cm^{-1}	7923		2844
vibrations, $\tilde{\nu}$/cm^{-1}	196, 313, 460, 524, 617, 631, 647, 772, 834, 889, 908, 948, 960, 1065, 1087, 1139, 1283, 1354, 1379, 1435, 1444, 2221, 2241, 2902, 2976, 2988, 2993, 3005 3075	208, 367, 411, 541 608, 711, (706*i*), 839, 877, 921, 929, 956, 1038, 1048, 1153, 1186, 1328, 1363, 1423, 1432, 1444, 1992, 2053, 2909, 2986, 3006, 3011, 3051 3102	190, 330, 482, 621, 741, 791, 881, 928, 1019, 1068, 1160, 1185, 1276, 1306, 1350, 1356, 1427, 1439, 1446, 2008, 2865, 2905, 2910, 2912 2912, 2954, 2997, 2999
rotational constants/cm^{-1}	0.357, 0.146, 0.122	0.382 0.128 0.110	0.817, 0.077, 0.074
internal rotor constants/cm^{-1}	5.482 ($\sigma = 3$)	5.434 ($\sigma = 3$)	5.486 ($\sigma = 3$), 0.650 ($\sigma = 1$)
symmetry number, enantiomers	1, 2	1, 2	1, 1

[a] Molecular structures and vibrational frequencies (0.9496 scaling factor)[24] are based on MP2/6-311G(d,p). Critical energies were taken from Table 2. Corresponding RRKM data for all other siliranes are given in the Supporting Information.

TABLE 4: Correlation Scheme and Molecular Parameters for the Simplified SACM Model of 2-Methylsilirane Decomposition, $CH_3-C_2SiH_5 + M \rightarrow SiH_2 + C_3H_6 + M$[a]

2-methylsilirane	$\tilde{\nu}(CH_3-C_2SiH_5)$	correlation	assignment
vibrations/cm^{-1}	196	→1.542	$A(C_3H_6)$
	313	403	$\tilde{\nu}(C_3H_6)$ (CCC bend)
	460	→3.786	$C(SiH_2)$
	524	→0.310	$B(C_3H_6)$
	617	→8.219	$A(SiH_2)$
	631	reaction coordinate	
	647	552	$\tilde{\nu}(C_3H_6)$
	772	→7.018	$B(SiH_2)$
	834	894	$\tilde{\nu}(C_3H_6)$
	889	974	$\tilde{\nu}(C_3H_6)$
	908	1013	$\tilde{\nu}(SiH_2)$
	948	1021	$\tilde{\nu}(C_3H_6)$
	960	861	$\tilde{\nu}(C_3H_6)$
	1065	902	$\tilde{\nu}(C_3H_6)$
	1087	1620	$\tilde{\nu}(C_3H_6)$ (C═C stretch)
	1139	1138	$\tilde{\nu}(C_3H_6)$
	1283	1257	$\tilde{\nu}(C_3H_6)$
	1354	1348	$\tilde{\nu}(C_3H_6)$
	1379	1389	$\tilde{\nu}(C_3H_6)$
	1435	1422	$\tilde{\nu}(C_3H_6)$
	1444	1438	$\tilde{\nu}(C_3H_6)$
	2221	2047	$\tilde{\nu}(SiH_2)$
	2241	2040	$\tilde{\nu}(SiH_2)$
	2902	2913	$\tilde{\nu}(C_3H_6)$
	2976	2985	$\tilde{\nu}(C_3H_6)$
	2988	3015	$\tilde{\nu}(C_3H_6)$
	2993	3004	$\tilde{\nu}(C_3H_6)$
	3005	3027	$\tilde{\nu}(C_3H_6)$
	3075	3111	$\tilde{\nu}(C_3H_6)$
internal rotor constant/cm^{-1} ($\sigma = 3$)	5.482 ($\tilde{\nu} = 234$)	6.130 ($\tilde{\nu} = 189$)	C_3H_6
$A(CH_3-C_2SiH_5)$ (K rotor)	0.357	→0.271	$C(C_3H_6)$
critical energy/cm^{-1}	$D_e = 15678$	$E_0 = 14223$	
Morse parameter, anisotropy ratio	$\beta = 2.569$	$\alpha/\beta = 0.560$	
$CH_3-C_2SiH_5$ rotational constants/cm^{-1}		0.357, 0.146, 0.122	$\sigma = 1$, prolate
C_3H_6 rotational constants/cm^{-1}		1.542, 0.310, 0.271	$\sigma = 1$, "sphere"
SiH_2 rotational constants/cm^{-1}		8.219, 7.018, 3.786	$\sigma = 2$, "sphere"
$CH_3-C_2SiH_5$ structure	quasi-triatomic, $m = 15.0$ (CH_3, a), 27.0 (C_2H_3, b), and 30.1 (SiH_2, c) $r_{ab} = 2.144$ Å, $r_{bc} = 1.785$ Å, $\angle_{cba} = 104.1°$		
Lennard-Jones parameters (Ar, SF_6, $CH_3-C_2SiH_5$)		σ/Å = 3.47, 5.20, 5.6	ε/K = 114, 212, 363

[a] Molecular structures and vibrational frequencies (0.9496 scaling factor)[24] are based on MP2/6-311G(d,p) and the critical energy on G3 ab initio calculations.[2021] Corresponding SACM data for all other siliranes are given in the Supporting Information.

rate constant k_∞ is determined by the respective $k_a(E)$ values alone and therefore does not depend on the isomerization process.

More detailed falloff calculations have been based on weak collision master equation (ME) simulations. The ME was solved using a single exponential collision model with the average energy removal parameter $\langle \Delta E_{down} \rangle$ as the sole fitting parameter. Numerical ME simulations were performed with an energy grain size of $\Delta E = 10$ cm^{-1} using a modified ME-subroutine from the UNIMOL program suite.[29] Rotational effects were approximately taken into account by using suitably averaged $k(E, J)$ values. For high J numbers, an increasing amount of external rotational energy is available to cross the dissociation barrier causing the effective dissociation barrier to decrease with

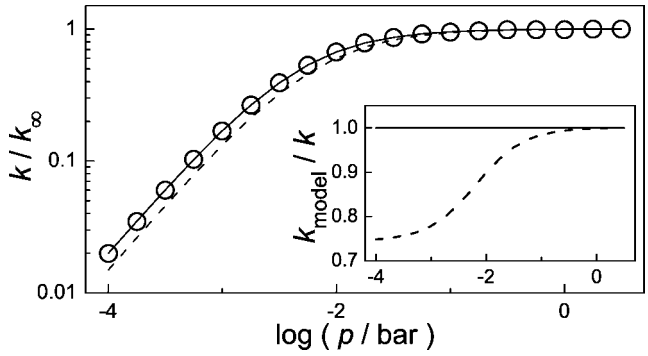

Figure 6. Influence of the silirane/ethylsilylene isomerization on the overall rate constant of the addition reaction $SiH_2 + C_2H_4$. Falloff curves based on the extended Lindemann−Hinshelwood model including isomerization (circles), on a model using an efficient decomposition rate constant (solid curve), and on a simple recombination model neglecting isomerization (dashed curve). The inset illustrates the relative deviations of the approximate models.

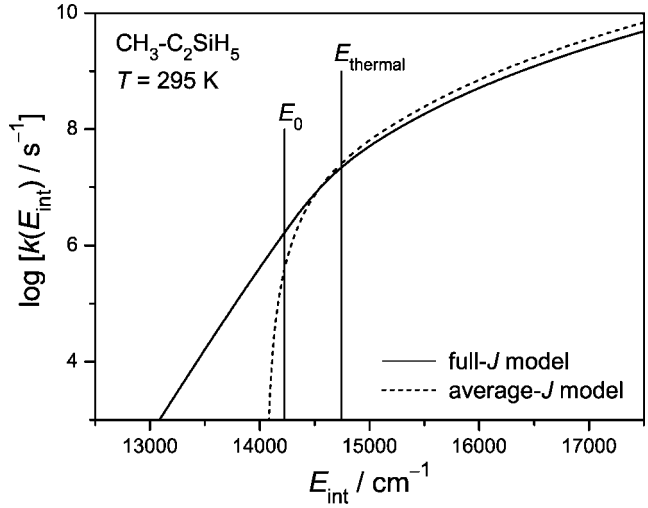

Figure 7. Calculated specific rate constants for the dissociation of 2-methylsiliran ($CH_3-C_2SiH_5$) based on two different treatments of the external rotation contribution (see text). Full-J model: $\alpha/\beta = 0.560$ ($k_\infty = 3.3 \times 10^{-13}$ s^{-1}). Average-J model: $\alpha/\beta = 0.612$ ($k_\infty = 3.3 \times 10^{-13}$ s^{-1}). E_0 corresponds to the energy barrier ($J = 0$), and $E_{thermal}$ is the initial internal energy E_{int} of the association complex including thermal energy of the reactant.

increasing J. To account for this effective reaction barrier, for every J the $k(E, J)$ values were shifted along the energy axis and were then averaged over the thermal rotational distribution yielding temperature-dependent $k(E, T)$ values (full-J model). In Figure 7, a typical $k(E, T = 295$ K) curve is shown for 2-methylsilirane decomposition (solid curve). E_0 specifies the $J = 0$ energy barrier, and $E_{thermal}$ corresponds to the thermally averaged internal energy of the reactant. In principle, having no fixed energy barriers, for very high rotational excitation, a nonzero reaction probability at an internal energy of $E = 0$ is possible. The full-J model appropriately accounts for the higher dissociation probability of high J states but implicitly assumes a thermal distribution of the rotational states at all pressures. Toward lower pressures, high internal energy states start to get depleted, and the relative importance of high J states for the observed total rate constant increases. Therefore, by assuming an immediate repopulation of these high J level states (even at $p = 0$), the full-J model must eventually fail at very low pressures. However, since rotational relaxation is known to be significantly faster than vibrational energy transfer, these inaccuracies are expected to occur at pressures much lower than the pressures used in this work, which were quite close to the high-pressure limit.

An alternative approximate J-averaging procedure is possible. Within the average-J model, specific rate constants $k(E, J)$ and also the effective reaction barriers $E_0(J)$ are averaged over the thermal J distribution separately. The obtained results are very similar to a model that simply assumes $k(E, J_{average})$ values together with the corresponding effective barrier $E_0(J_{average})$. An advantage of this model is that it retains a more intuitive fixed reaction barrier, but the model does not properly account for the higher reaction probability of high J states compared to low J states. Therefore, systematically lower k_∞ values are predicted that have to be compensated by adjusting other model parameters, i.e., the anisotropy ratio α/β in the case of SACM calculations. In Figure 7, the dashed curve reflects a $k(E, T = 295$ K) curve that was obtained with $\alpha/\beta = 0.612$ based on the average-J model. It yields the same k_∞ value as the full-J model with $\alpha/\beta = 0.560$. Using $\alpha/\beta = 0.560$ together with the average-J model would have resulted in a 32% lower k_∞.

In principle, the approximate and somewhat ambiguous J-averaging procedure, which is necessary to perform a 1-D internal energy-grained ME simulation, can be avoided by applying full 2-D ME models. However, more laborious 2-D ME simulations with full angular momentum conservation are beyond the scope of this paper. They would have required the modeling of rotational energy transfer probabilities, and thus at least one more uncertain parameter would have been necessary.[10,30]

In the following, theoretical falloff curves were calculated based on the full-J model using the anisotropy ratio α/β and the average energy removal parameter $\langle\Delta E_{down}\rangle$ as the sole fitting parameters. In the case of ethene, specific rate constants have been multiplied by $x_{cycl} = 0.74$ to account for the fast isomerization process. α/β was used to fit the extrapolated k_∞ value, and $\langle\Delta E_{down}\rangle$ was adjusted to reproduce the falloff curvature. Note that both the critical energy E_0 and all the structural parameters of the reactants and products were left unchanged from their ab initio values. Modeling parameters and results are listed in Table 5 and are plotted in Figures 5 and 8 together with experimental data. Comprehensive tables of falloff curve data and equilibrium constant values, which were used to convert unimolecular decomposition into recombination rate constants, can be found in the Supporting Information.

5. Discussion

Experimental room-temperature data obtained in this work (ethene, propene, *t* -butene, Ar buffer gas) and *i*-butene literature data (SF_6 buffer gas) taken from Al-Rubaiey et al.[9] are compared with SACM modeling results in Figure 5. More temperature-dependent literature data are shown for ethene, propene, and *i*-butene (SF_6 buffer gas) in Figure 8 and were taken from Al-Rubaiey and Walsh[8] and Al-Rubaiey et al.[9] In Walsh and co-workers studies, the SiH_2 + alkene reactions were investigated under pseudofirst-order reaction conditions, and SiH_2 radicals were detected by means of narrow-bandwidth laser absorption using a reaction cell equipped with multipass optics. Although the used phenylsilane precursor concentrations (10^{-10} mol/cm^3 at room temperature, up to 10^{-9} mol/cm^3 at high temperatures) were higher than in the present work and static reactors were used instead of a flow reactor, these studies are comparable to our work and the results can be used to build a suitable combined database. Overall, the SACM models are capable of a consistent and reliable prediction of both the absolute rate constants and the pressure and temperature dependences of the

TABLE 5: High-Pressure Limiting Room-Temperature Recombination Rate Constants (k_∞/cm^3·mol^{-1}·s^{-1}) = (A/cm^3·mol^{-1}·s^{-1}) × (T/K)^n (295 ≤ T/K ≤ 600), SACM Anisotropy Ratios α/β, Energy Transfer Parameters ⟨ΔE_{down}⟩ (Exponential Model), and Lennard-Jones Collision Numbers Z_{LJ}

		k_∞			⟨ΔE_{down}⟩/cm^{-1}		Z_{LJ}/(cm^3·mol^{-1}·s^{-1})	
reactants	α/β	(cm^3·mol^{-1}·s^{-1})	A	n	Ar	SF_6	Ar	SF_6
$SiH_2 + C_2H_4$	0.560	1.3×10^{14}	1.9×10^{14}	−0.065	250	600	2.5×10^{14}	3.0×10^{14}
$SiH_2 + C_3H_6$	0.560	2.0×10^{14}	1.3×10^{14}	0.075	250	600	2.6×10^{14}	3.1×10^{14}
$SiH_2 + i$-C_4H_8	0.515	1.8×10^{14}	1.8×10^{14}	0	250	600	2.8×10^{14}	3.1×10^{14}
$SiH_2 + t$-C_4H_8	0.539	1.5×10^{14}	4.6×10^{13}	0.21	250	600	2.8×10^{14}	3.1×10^{14}

addition reactions. For a class of similar reactions, comparable anisotropy ratios can be expected. Hence, the obtained small range of α/β values used in the simulations, 0.515 < α/β < 0.560 (Table 5), indicate a reliable input data set for the SACM models, i.e., critical energies and structural parameters. Also, the absolute values of the anisotropy ratios, which are close to the "standard" value of 0.5, are well within expectations. Moreover, it was possible to model all falloff data using the same average energy removal parameters of ⟨ΔE_{down}⟩ = 250 cm^{-1} for Ar and 600 cm^{-1} for SF_6 as the buffer gas. Walsh and co-workers, based on more approximate RRKM treatment of the SiH_2 addition reactions, reported somewhat higher values of 400 cm^{-1} for Ar and 800 cm^{-1} for SF_6.[4,9] Remaining discrepancies in the case of ethene, i.e., somewhat too high modeled rate constants at low pressures (see Figure 5), are most likely due to reasons other than the assumed ⟨ΔE_{down}⟩ value and will be discussed below. For example, a ME calculation based on ⟨ΔE_{down}⟩ = 100 cm^{-1} did not significantly improve the agreement between the theoretical model and the experimental ethene data.

All extrapolated high-pressure limiting room-temperature recombination rate constants are close to the corresponding Lennard-Jones collisional numbers, $Z_{LJ} = (2.5-3.1) \times 10^{14}$ cm^3·mol^{-1}·s^{-1}. In spite of the comparable values obtained for the different alkenes, $1.3 \times 10^{14} < k_\infty/(\text{cm}^3\cdot\text{mol}^{-1}\cdot\text{s}^{-1}) < 2.0 \times 10^{14}$, a trend of the rate constants according to k_∞(ethene) < k_∞(propene) ≈ k_∞ (*i*-butene) > k_∞ (*t*-butene) is discernible. This trend is consistent with a heuristic interpretation that the measured rate constant reflects the interplay of two effects. On one hand, alkyl substitution should enhance the electrophilic SiH_2 attack (+I inductive effect), and on the other hand, with bulkier substituents or with two substituents present, steric effects should become more important and hinder SiH_2 attack. However, given the comparable values of the high-pressure rate constants and an estimated error of k_∞ in the order of ± (15−25)% (data scatter and extrapolation error), it is clear that the trend is barely significant and should not be overinterpreted.

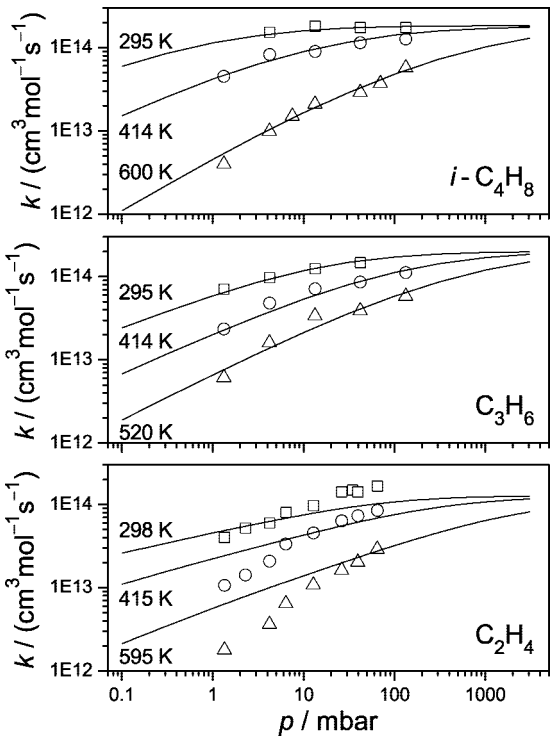

Figure 8. Temperature dependence of modeled falloff curves (SF_6 buffer gas, ⟨ΔE_{down}⟩ = 600 cm^{-1}) in comparison with literature data. $SiH_2 + C_2H_4$ data from Al-Rubaiey and Walsh;[8] $SiH_2 + C_3H_6$ data from Al-Rubaiey et al.[9] (scaled by a factor of 0.89); $SiH_2 + i$-C_4H_8 data from Al-Rubaiey et al.[9]

Using He as buffer gas, Chu et al.[31] reported a room-temperature rate constant of 7.2×10^{13} cm^3·mol^{-1}·s^{-1} for the reaction $SiH_2 + C_3H_6$ at p = 6.7 mbar. Reproducing this value with our model yields ⟨ΔE_{down}⟩ = 185 cm^{-1} for He, consistent with the general trend of ⟨ΔE_{down}⟩(He) ≤ ⟨ΔE_{down}⟩(Ar). Moreover, as can be seen in Figure 8 for propene and *i*-butene, nearly perfect agreement is also found for the temperature dependences of the falloff curves reported by Al-Rubaiey et al.[9] For propene, the anisotropy ratio was determined from our own room-temperature data yielding approximately 10% higher k_∞ values than would have been obtained based on the data of Al-Rubaiey et al. This small discrepancy is well within the error limits, and therefore, for the comparison with our theoretical prediction, the experimental data of Al-Rubaiey were scaled by a factor of 0.89 in Figure 8. As is common for simple recombination reactions, the falloff is more pronounced at high temperatures, but the limiting high-pressure rate constant is only weakly dependent on temperature. Predicted temperature-dependent high-pressure rate constants according to $k_\infty = A \times T^n$ are given in Table 5. With 0.21 ≥ n ≥ −0.063, all reactions are more or less temperature independent over the temperature range 600 K ≥ T ≥ 295 K. Slightly more distinctive (negative) temperature dependences of −0.6 ≥ n ≥ −0.8 reported by Al-Rubaiey et al.[9] can be ascribed to the more approximate RRKM model used by these authors and in particular to the neglect of rotational effects.

In view of the very good agreement of the SACM model with experimental data found for propene, *i*-butene, and *t*-butene, the less satisfying modeling in the case of ethene is surprising. From Figures 5 and 8, it becomes clear that the model approximately reproduces the absolute values and the temperature dependence of the k_∞ values, but the falloff curvature is noticeably underestimated, yielding too high rate constants at lower pressures. A more detailed comparison of our room temperature results with literature data is shown in Figure 9. The different data sets have been measured with Ar or He as the buffer gas and, despite the expected slightly lower collision efficiency of He, should be comparable. Up to pressures of p ≤ 10 mbar, good agreement is found between our data (filled circles, Ar), the data of Chu et al.[31] (open triangles, He), and

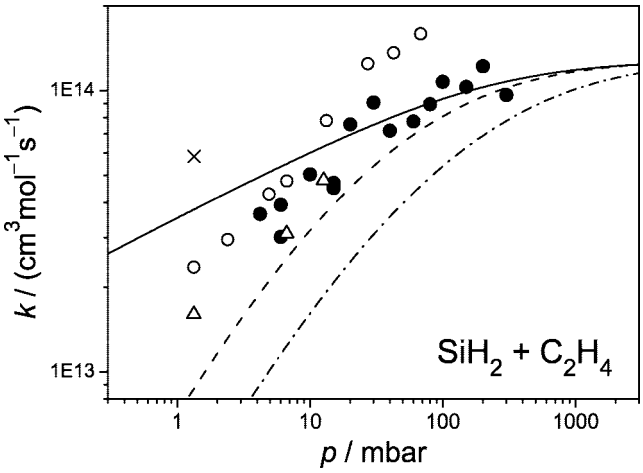

Figure 9. Comparison of experimental room-temperature rate constant data with kinetic modeling results for the reaction $SiH_2 + C_2H_4$. (●) this work (Ar, $T = 295$ K); (○) Al-Rubaiey et al.[4] (Ar, 298 K); (Δ) Chu et al.[31] (He, 298 K); (×) Inoue and Suzuki[32] (He, 298 K). SACM modeling results: (—) full-J model with $\alpha/\beta = 0.56$ and $\langle\Delta E_{down}\rangle$(Ar) = 250 cm^{-1}; (—•—•) average-J model with $\alpha/\beta = 1.0$ and $\langle\Delta E_{down}\rangle$(Ar) = 250 cm^{-1}; (- - - -) average-J model with $\alpha/\beta = 1.0$ and $\langle\Delta E_{down}\rangle$(Ar) = 1000 cm^{-1}.

the data of Al-Rubaiey et al.[4] (open circles, Ar). The single measurement of Inoue and Suzuki[32] in He at $p = 1.33$ mbar, which is based on SiH_2 detection using laser-induced fluorescence, corresponds to a 3 times faster rate constant and can be considered as an outlier. At pressures $p > 10$ mbar, the data of Al-Rubaiey et al. start to diverge from our own data for unknown reasons and are already a factor of 1.8 higher at $p =$ 68 mbar. The solid curve in Figure 9 represents our SACM fit using $\alpha/\beta = 0.56$ and corresponds to a high-pressure limiting rate constant of $k_\infty = 1.3 \times 10^{14}$ $cm^3 \cdot mol^{-1} \cdot s^{-1}$. A significantly higher value of $k_\infty = 2.1 \times 10^{14}$ $cm^3 \cdot mol^{-1} \cdot s^{-1}$ as recommended by Walsh and co-workers[4,8] would require an anisotropy ratio of $\alpha/\beta = 0.61$ and thus is less compatible with our SACM model. To assess the influence of the rotational effects, falloff curves have been also evaluated based on the average-J model and are shown as dash-dotted and dashed curves in Figure 9. Here, an unrealistic ratio of $\alpha/\beta = 1.00$ was necessary to reproduce the extrapolated k_∞ value. Moreover, the obtained falloff curve with $\langle\Delta E_{down}\rangle = 250$ cm^{-1} (dash-dotted curve) fails to reproduce the experimentally observed pressure dependence. Even increasing the energy removal parameter to an unrealistic value of $\langle\Delta E_{down}\rangle = 1000$ cm^{-1} (dashed curve) does not yield reasonable falloff rate constants. The marked differences of the two different rotational models reveal a strong influence of rotational effects and, justified by the much better agreement of the full-J model, point out the importance of high J states.

Remaining discrepancies in the modeling of the falloff curves for ethene can have several explanations. First, in comparison with the higher alkenes, ethene exhibits the loosest transition state making its modeling more sensitive to model deficiencies, e.g., the modeling of the dissociation coordinate using a simple Morse potential. Second, in contrast to the other alkenes, the fast silirane/ethylsilylene isomerization process had to be taken into account. The applied correction procedure is based on a simple Lindemann−Hinshelwood model, and its use for detailed weak collision ME modeling may have introduced additional uncertainties. Third, ab initio model parameters entering the SACM model play a significant role. For example, a variation of the critical energy E_0 by ± 10 kJ/mol induces a systematic shift of the calculated falloff curve, although its shape and the limiting high-pressure rate constant are not significantly different. Therefore, in view of the consistent ab initio model used for all alkenes and the very good agreement of the model with the propene, *i*-butene, and *t*-butene experiments, we believe that possible uncertainties of the input parameters are less significant. As a fourth reason, as was outlined above, the modeling of the rotational effects turned out to be very important. A comparison of the falloff curves obtained with the two different rotational models shown in Figure 9 reveals that the experimental data fall in between these two limiting cases. This might be an indication that toward lower pressures the assumption of an instantaneous rotational relaxation (full-J model) starts to fail. A final possible explanation for the deviation is associated with an additional weakly bound intermediate complex in the entrance valley of the recombination reaction potential. Such complexes can play a significant role for the overall recombination reactions and have been reported for SiH_2 insertion reactions.[33] However, since the search for such complexes should be based on higher level ab initio calculations than that used in this work, they cannot be completely ruled out.

A differentiation between the mentioned possible sources of error is difficult. Probably the approximate treatment of the rotational effects and/or the interfering isomerization are the main reasons for the remaining discrepancies of the theoretical model and the ethene experiments at low pressures. More detailed models based on accurate dissociation potentials and sophisticated theories of recombination reactions combined with 2-D ME simulations that properly account for the isomerization process are needed to gain a deeper insight into peculiarities of the reaction system. Since our intent was the application of straightforward modeling procedures, such a detailed analysis would have been beyond the scope of this paper. 2-D ME simulations are at present still in their infancy.

6. Conclusion

Using CRDS as a sensitive detection method for SiH_2 radicals, the rate constants of several fast SiH_2 addition reactions have been measured over a wide range of pressures. An interfering laser bandwidth effect could properly be taken into account by simulating the obtained nonexponential ringdown curves based on the eSKaR model.

All studied reactions proceed close to collisional frequency and, in agreement with ME simulations, showed a pronounced pressure dependence. Overall, the approach of using G3 energies and MP2 structural parameters taken from ab initio calculations as input for simplified SACM/ME calculations has been shown to permit a consistent rate constant modeling. Using an average anisotropy ratio of $\alpha/\beta = 0.54$, the calculations can be easily extended to other SiH_2 addition reactions and make possible a reliable estimate of temperature- and pressure-dependent recombination rate constants. A more detailed theoretical treatment appears to be needed in the case of the reaction $SiH_2 + C_2H_4$ to clarify remaining discrepancies observed at low total pressures.

Acknowledgment. We would like to thank the Deutsche Forschungsgemeinschaft and the Fonds der Chemischen Industrie for the support of this work.

Supporting Information Available: RRKM and SACM input parameters, modeled falloff data, ab initio energies, and transition state structures. This material is available free of charge via the Internet at http://pubs.acs.org.

References and Notes

(1) Gaspar, P. P. *Reactive Intermediates: Silylenes*; Jones, M., Moss, R. A. Eds.; Wiley: New York, 1985.

(2) Tang, Y. N. *Reactive Intermediates: Reactions of Silicon Atoms and Silylenes*; Abramovitch, R. A. Ed.; Plenum: New York, 1982.

(3) Jutzi, P.; Schubert, U. *Silicon Chemistry - From Molecules to Extended Systems*; John Wiley & Sons: Chichester, UK, 2003.

(4) Al-Rubaiey, N.; Frey, H. M.; Mason, B. P.; McMahon, C.; Walsh, R. *Chem. Phys. Lett.* **1993**, *204*, 301.

(5) Jasinski, J. M.; Becerra, R.; Walsh, R. *Chem. Rev.* **1995**, *95*, 1203.

(6) Becerra, R.; Walsh, R. *Research in Chemical Kinetics: Kinetics & mechanisms of silylene reactions: A prototype for gas-phase acid/base chemistry*; Compton, R. G., Hancock, G. Eds.; Elsevier: Amsterdam, 1995; Vol. 3.

(7) Becerra, R.; Walsh, R. *Phys. Chem. Chem. Phys.* **2007**, *9*, 2817.

(8) Al-Rubaiey, N.; Walsh, R. *J. Phys. Chem.* **1994**, *98*, 5303.

(9) Al-Rubaiey, N.; Carpenter, I. W.; Walsh, R.; Becerra, R.; Gordon, M. S. *J. Phys. Chem. B* **1998**, *102*, 8564.

(10) Gilbert, R. G.; Smith, S. C. *Theory of Unimolecular and Recombination Reactions*; Blackwell Scientific Publications: Oxford (U.K.), 1990.

(11) Troe, J. *J. Chem. Phys.* **1981**, *75*, 226.

(12) Sengupta, D.; Nguyen, M. T. *Mol. Phys.* **1996**, *89*, 1567.

(13) Skancke, P. N.; Hrovat, D. A.; Borden, W. T. *J. Am. Chem. Soc.* **1997**, *119*, 8012.

(14) Al-Rubaiey, N.; Becerra, R.; Walsh, R. *Phys. Chem. Chem. Phys.* **2002**, *4*, 5072.

(15) Guo, Y. Q.; Fikri, M.; Friedrichs, G.; Temps, F. *Phys. Chem. Chem. Phys.* **2003**, *5*, 4622.

(16) Friedrichs, G. Z. *Phys. Chem.* **2008**, *222*, 31.

(17) Baggott, J. E.; Frey, H. M.; Lightfoot, P. D.; Walsh, R. *Chem. Phys. Lett.* **1986**, *125*, 22.

(18) Friedrichs, G.; Colberg, M.; Fikri, M.; Huang, Z.; Neumann, J.; Temps, F. *J. Phys. Chem. A* **2005**, *109*, 4785.

(19) Brown, S. S.; Ravishankara, A. R.; Stark, H. *J. Phys. Chem. A* **2000**, *104*, 7044. and *J. Phys. Chem. A*, **2000**, *104*, 8600.

(20) Curtiss, L. A.; Raghavachari, K.; Redfern, P. C.; Rassolov, V.; Pople, J. A. *J. Chem. Phys.* **1998**, *109*, 7764.

(21) Frisch, M. J.; Trucks, G. W.; Schlegel, H. B.; Scuseria, G. E.; Robb, M. A.; Cheeseman, J. R.; Montgomery, J. A., Jr.; Vreven, T.; Kudin, K. N.; Burant, J. C.; Millam, J. M.; Iyengar, S. S.; Tomasi, J.; Barone, V.; Mennucci, B.; Cossi, M.; Scalmani, G.; Rega, N.; Petersson, G. A.; Nakatsuji, H.; Hada, M.; Ehara, M.; Toyota, K.; Fukuda, R.; Hasegawa, J.; Ishida, M.; Nakajima, T.; Honda, Y.; Kitao, O.; Nakai, H.; Klene, M.; Li, X.; Knox, J. E.; Hratchian, H. P.; Cross, J. B.; Bakken, V.; Adamo, C.; Jaramillo, J.; Gomperts, R.; Stratmann, R. E.; Yazyev, O.; Austin, A. J.; Cammi, R.; Pomelli, C.; Ochterski, J. W.; Ayala, P. Y.; Morokuma, K.; Voth, G. A.; Salvador, P.; Dannenberg, J. J.; Zakrzewski, V. G.; Dapprich, S.; Daniels, A. D.; Strain, M. C.; Farkas, O.; Malick, D. K.; Rabuck, A. D.; Raghavachari, K.; Foresman, J. B.; Ortiz, J. V.; Cui, Q.; Baboul, A. G.; Clifford, S.; Cioslowski, J.; Stefanov, B. B.; Liu, G.; Liashenko, A.; Piskorz, P.; Komaromi, I.; Martin, R. L.; Fox, D. J.; Keith, T.; Al-Laham, M. A.; Peng, C. Y.; Nanayakkara, A.; Challacombe, M.; Gill, P. M. W.; Johnson, B.; Chen, W.; Wong, M. W.; Gonzalez, C.; Pople, J. A. *Gaussian 03, revision 0.01*, Gaussian, Inc.: Wallingford, CT, 2004.

(22) Roggenbuck, J. Theoretische Behandlung komplexbildender bimolekularer Reaktionen in der Gasphase. Die Reaktionen $^3CH_2 + NO$ und $SiH_3 + O_2$, Ph.D. thesis Universität Kiel, 2000.

(23) Forst, W. *Unimolecular Reactions*; Cambridge University Press: Cambridge (U.K.), 2003.

(24) Scott, A. P.; Radom, L. *J. Phys. Chem.* **1996**, *100*, 16502.

(25) Quack, M.; Troe, J. *Ber. Bunsenges. Phys. Chem.* **1974**, *78*, 240.

(26) Troe, J. *J. Chem. Phys.* **1983**, *79*, 6017.

(27) Reid, R. C.; Prausnitz, J. M.; Poling, B. E. *The Properties of Gases & Liquids*, 4th ed.; McGraw-Hill: New York, 1988.

(28) Krasnoperov, L. N.; Niiranen, J. T.; Gutman, D.; Melius, C. F.; Allendorf, M. D. *J. Phys. Chem.* **1995**, *99*, 14347.

(29) Gilbert, R. G.; Smith, S. C.; Jordan, M. J. T. *UNIMOL program suite (calculation of fall-off curves for unimolecular and recombination reactions), 1993, available from the authors*; School of Chemistry, Sydney University, NSW: Australia, 2006.

(30) Fernández-Ramos, A.; Miller, J. A.; Klippenstein, S. J.; Truhlar, D. G. *Chem. Rev.* **2006**, *106*, 4518.

(31) Chu, J. O.; Beach, D. B.; Jasinski, J. M. *J. Phys. Chem.* **1987**, *91*, 5340.

(32) Inoue, G.; Suzuki, M. *Chem. Phys. Lett.* **1985**, *122*, 361.

(33) Becerra, R.; Carpenter, I. W.; Gordon, M. S.; Roskop, L.; Walsh, R. *Phys. Chem. Chem. Phys.* **2007**, *9*, 2121.

JP8012128